Frequency-Hopping MIMO Radar-Based Communications: An Overview

Kai Wu, J. Andrew Zhang, *Senior Member, IEEE*, Xiaojing Huang, *Senior Member, IEEE*, and Y. Jay Guo, *Fellow, IEEE*

***Abstract*—Enabled by the advancement in radio frequency technologies, the convergence of radar and communication systems becomes increasingly promising and is envisioned as a key feature of future sixth-generation networks. Recently, the frequency-hopping (FH) MIMO radar is introduced to underlay dual-function radar-communication (DFRC) systems. Superior to many previous radar-centric DFRC designs, the symbol rate of FH-MIMO radar-based DFRC (FH-MIMO DFRC) can exceed the radar pulse repetition frequency. However, many practical issues, particularly those crucial to achieving effective data communications, are unexplored or unsolved. To promote the awareness and general understanding of the novel DFRC, this article is devoted to providing a timely introduction of FH-MIMO DFRC. We comprehensively review many essential aspects of the novel DFRC: channel/signal models, signaling strategies, modulation/demodulation processing and channel estimation methods, to name a few. We also highlight major remaining issues in FH-MIMO DFRC and suggest potential solutions to shed light on future research directions.**

***Index Terms*—Multi-Functional RF Systems (MFRFS), joint communication and radar/radio sensing (JCAS), dual-function radar-communication (DFRC), frequency hopping (FH), MIMO radar, frequency-agile radar (FAR), timing offset and channel estimation.**

I. Introduction

Enabled by the advancement in radio frequency (RF) technologies and signal processing, the convergence of multi-functional RF systems becomes increasingly promising and is envisioned as a key feature of future sixth-generation (6G) networks [1]. Among numerous RF systems, including wireless communications, radio sensing, mobile computing, localization, etc., the former two have achieved significant progress recently on their integration. This is evidenced by several timely overview, survey and tutorial papers [2]–[5].

Driven by the spectrum scarcity and cost saving, co-existence between radar and communications has been investigated in the past few years, with focus on mitigating the interference between the two RF functions [2]. Thanks to the shared commonalities in terms of signal processing algorithms, hardware and, to some extent, system architecture, joint communication and radar/radio sensing (JCAS), also referred to as dual-function radar-communication (DFRC), is emerging as an effective solution for integrating wireless communication and radio sensing [3]. Substantially different from the co-existence of the two RF functions, JCAS/DFRC aims to design and use a single transmitted signal for both communication and sensing, enabling a majority of the transmitter modules and receiver hardware to be shared.

The design of JCAS/DFRC can be communication-centric or radar-centric [4]. The former performs radar sensing using ubiquitous communication signals, e.g., IEEE 802.11p [6] and IEEE 802.11ad [7], whereas the later embeds information bits into existing radar waveform or specifically optimized dual-function waveforms [4]. Regarding the communication-centric JCAS, it is worth mentioning a recently proposed perceptive mobile network (PMN) [3]. Integrating sensing function into mobile networks, the PMN is envisaged to revolutionize the future fifth-generation (5G) and 6G networks by offering ubiquitous sensing capabilities for numerous smart applications, such as smart city/factory. Compared with the communication-centric counterpart, radar-centric designs, which has also been typically referred to as DFRC, generally have superior radar sensing performance, given the sensing-dedicated waveform.

Many recent DFRC designs lean towards using multiple-input multiple-output (MIMO) radar [4], [5], [8], potentially due to the following reasons. *First*, MIMO radar has gained the increasing popularity in the radar community given its advantages of better spatial resolution, improved interference rejection capability, improved parameter identifiability and enhanced flexibility in beam pattern design, as compared with the conventional (phased) array radar [9]. *Second*, in addition to the spatial degree-of-freedom (DoF), MIMO radar also provides extra DoF in the waveform, when embedding communication information. The spatial DoF can also be provided by a conventional array radar, while the waveform DoF cannot. The waveform DoF provided by MIMO radar enables more information to be embedded for DFRC and higher communication data rates to be achieved [4], [5].

In the context of DFRC, some researchers optimize the beam pattern of a MIMO radar to perform conventional modulations, e.g., phase shift keying (PSK) and amplitude shift keying, by designing the sidelobes in the MIMO radiation patterns. Other researchers optimize radar waveforms to perform non-traditional modulations, such as waveform shuffling and code shift keying. An overview of different signaling strategies/schemes based on MIMO radars can be found in [5]. As popularly used in the literature, the term, signaling strategy/scheme, is referred to as the way communication information is embedded in the radar waveform. Most previ-

Manuscript received September 29th, 2020. This work is partially funded by the NSW Defence Innovation Network and the NSW State Government through Pilot Project grant DINPP-19-20 10.01

K. Wu, J. A. Zhang, X. Huang and Y. J. Guo are with the Global Big Data Technologies Centre, University of Technology Sydney, Sydney, NSW 2007, Australia (e-mail: kai.wu@uts.edu.au; andrew.zhang@uts.edu.au; xiaojing.huang@uts.edu.au; jay.guo@uts.edu.au).

ous DFRC works by embedding one communication symbol within one or multiple radar pulses. The symbol rate is hence limited by radar pulse repetition frequency (PRF).

In some recently reported research [10]–[15], frequency-hopping MIMO (FH-MIMO) radar is introduced to DFRC, which breaks the above limit and substantially increases the communication symbol rate to multiples of (e.g., 15 times) PRF. Pioneering in conceiving the novel DFRC architecture based on FH-MIMO radar (FH-MIMO DFRC), the research reported in [10]–[15] focuses on analyzing the impact of information modulation on the radar ranging performance. In these works, little attention is paid to effective implementation of data communications. Some later research reported in [16]–[18] develops methods to address the practical issues, e.g., channel estimation and synchronization, in FH-MIMO DFRC.

Motivated by the rapidly increasing interest in DFRC and the lack of awareness and general understanding of FH-MIMO DFRC, this article aims to provide a timely introduction of the novel DFRC architecture. We start by discussing the potential applications and channel scenarios of FH-MIMO DFRC and also the commonly used signal model in the literature. Then, we survey the existing signaling strategies for FH-MIMO DFRC, illustrate their modulation and demodulation methods, and also compare the signaling strategies from various aspects. We further discuss the issue of channel estimation in FH-MIMO DFRC and report recently developed solutions. Finally, we highlight the major unsolved issues in FH-MIMO DFRC and suggest potential solutions to shed light on future research directions. It is noteworthy that this article provides a better coverage on the communication aspects of FH-MIMO DFRC, which are rarely dealt with in prior articles.

II. Scenarios and Signal Model for FH-MIMO DFRC

FH-MIMO radar is pulse-based and hence is likely to be employed in applications requiring a large range coverage, such as long-range air-surveillance. Besides, such radar is generally placed at a certain height, e.g., several hundreds meters, above the sea level, looking beyond clutter areas, so as to reduce ground clutters and co-frequency interference from terrestrial wireless systems. Therefore, FH-MIMO DFRC is promising for providing ground-to-air (G2A) communications for different types of aircraft, as depicted in Fig. 1. The aircraft can be an unmanned aerial vehicle (UAV), a civilian aeroplane (CAP) or a high-altitude platform (HAP).

In addition to target detection/tracking, FH-MIMO DFRC allows a radar to perform secure, long-range, low-latency, and high-speed wireless broadband connections with aircraft or warships over very wide areas. (Note that if the radar is performing wide-area search with a directional beam, the high-speed communication link can be intermittent.) DFRC benefits radar by, for instance, allowing the sensing results, e.g., target information or radar imaging, to be shared with other (airborne or ground-based) radar nodes. More benefits of DFRC to both radar and communications are comprehensively summarized in several recent overview/survey papers [3]–[5]. We underline that, as not captured in the previous work, the G2A link

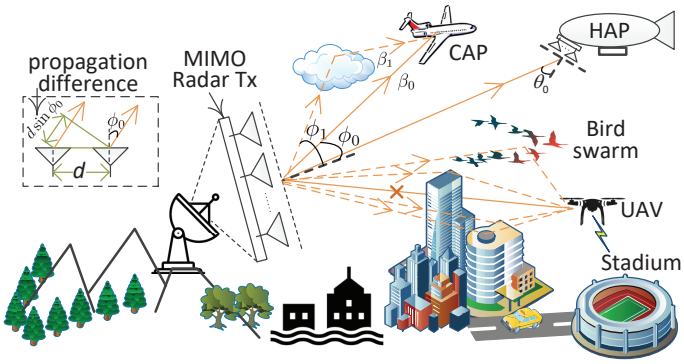

Fig. 1: A promising scenario of FH-MIMO DFRC, where an FH-MIMO radar is placed in a high-altitude platform to perform air surveillance and meanwhile communicate with an aircraft that can be an unmanned aerial vehicle (UAV), a civilian aeroplane (CAP) or a high-altitude platform (HAP). In the figure, ϕ_0 and ϕ_1 denote angles-of-departure (AoDs) of a line-of-sight (LoS) and a non-LoS (NLoS) path, respectively; β_0 and β_1 the path gains of the two paths; and θ_0 denotes the angle-of-arrival (AoA) of an LoS path.

provided by FH-MIMO DFRC may help support seamless wireless coverage, as expected to be realized by future 6G networks [1]. In particular, FH-MIMO DFRC can contribute to building the integrated space and terrestrial network (ISTN) which is envisioned to be at the core of 6G communication systems [19]. Employing satellites, in combination with FH-MIMO DFRC, may provide a more cost-effective solution to providing wireless connectivity for people and vehicles in remote rural areas and in the air, as well as at sea, as compared with the solutions solely relying on satellites. Against the above potential scenarios, we depict below the channel models suitable for FH-MIMO DFRC.

A. Channel Models Suitable for FH-MIMO DFRC

The channel distribution for FH-MIMO DFRC can vary with the altitude of an airborne user equipment (UE). The typical altitudes of UAVs, CAPs and HAPs are 10^3 m, 10×10^3 m and 20×10^3 m above the sea level, respectively [20]. Therefore, in FH-MIMO DFRC, the following flat-fading channel distributions are likely to be present. These channel models have been well-established in conventional data communications [21, Chapter 3].

1) Rayleigh channel is likely to exist between the radar and a UAV, particularly when the line-of-sight (LoS) path is blocked by a high-rise building and there exist numerous scattering paths; see Fig. 1.
2) Rician channel can be common between the radar and a CAP, where only few non-LoS (NLoS) paths are present and are possibly much weaker than the LoS path;
3) Additive white Gaussian noise (AWGN) channel can prevail between the radar and an HAP where the LoS dominates the channel with negligible NLoS paths.

The geometric Saleh-Valenzuela (SV) channel model [21], with flexible parameters, can be adapted for depicting the three distributions. For ease of illustration, assume that a single antenna is equipped at the UE, which is widely considered in the related works [10]–[17].

Consider that there are P scattering points contributing to P communication paths. Let p denote the index of the p-th ($p =$

$0, 1, \cdots, P-1$) path and β_p the path gain. Two paths, i.e., $p = 0$ and 1, between the radar transmitter and the aeroplane are illustrated in Fig. 1. The geometric SV channel model can be expressed as

$$\mathbf{b} = \sum_{p=0}^{P-1} \beta_p \mathbf{a}_M(u_p) \tag{1}$$

where $\mathbf{a}_M(u_p)$ denotes the M-dimensional steering vector of the radar transmitter array in the direction of u_p. Here, u_p (in radians) is referred to as the beamspace-domain angle-of-departure (AoD) which is different from the AoD ϕ_p (in degree) illustrated in Fig. 1. Considering the uniform linear array, the m-th element of $\mathbf{a}_M(u_p)$ is $e^{-\mathrm{j}mu_p}$ ($m = 0, 1, \cdots, M-1$). Next, we use path $p = 0$ to illustrate the relation between u_0 and ϕ_0. As illustrated in Fig. 1, the propagation paths from two adjacent antennas to a far-field receiver are different in path length, and the difference is given by $d \sin \phi_0$. This difference can be expressed as $d \sin \phi_0 / \lambda$ numbers of wavelength, as denoted by λ. Since each wavelength corresponds to a phase change of 2π, the difference in path length causes a phase difference of $2\pi d \sin \phi_0 / \lambda$ between the two signals transmitted by the adjacent antennas. To this end, we have $u_0 = 2\pi d \sin \phi_0 / \lambda$.

Depending on the values of P and β_p $\forall p$, the SV channel can be simplified to the three classical channels illustrated above. Letting p and $p' (\neq p)$ be indexes of different paths, the SV channel model can become: 1) Rayleigh channel for $P \gg 1$ and all the paths between the radar transmitter and UE receiver have similar path gains; 2) Rician channel for $P > 1$ and the LoS path, i.e., path $p = 0$, has greater path gain than the NLoS paths, as indexed by $\forall p' (\neq p)$; and 3) AWGN channel for $P = 1$. In essence, $P = 1$ indicates that the path gains of NLoS are so small that they are negligible compared with the path gain of the LoS. So far, most previous works only consider AWGN channels for FH-MIMO DFRC, with exceptions in, e.g., [17].

B. Signal Model

The FH-MIMO radar is based on fast frequency hopping. Namely, each pulse is divided into H sub-pulses, also referred to as hops [14]. A sinusoidal signal is transmitted in each hop, and the frequency of the sinusoidal signal changes randomly across hops and antennas, as illustrated in Fig. 2. Denote the radar bandwidth as B. By dividing the frequency band evenly into K sub-bands, each sub-band has the bandwidth of B/K. Out of the K centroid frequencies, $M (< K)$ frequencies are selected to be the hopping frequencies per hop, one for each antenna. Let k_{hm} denote the index of the sub-band selected by antenna m at hop h. To ensure the waveform orthogonality of FH-MIMO radar, the following constraints are imposed for the radar [9],

$$k_{hm} \neq k_{hm'} \ (\forall m \neq m', \ \forall h); \ \Delta \triangleq BT/K \in \mathbb{I}_+, \tag{2}$$

where m and m' are indexes of two different antennas, T is the time duration of a hop and $\mathbb{I}_+$ denotes the set of positive integers. The first constraint in (2) indicates that no two antennas use the same sub-band as hopping frequency. This is reflected in Fig. 2 through that the third digits in the table units along each column do not have identical values. The benefit of the second constraint is to be demonstrated shortly.

At hop h, the m-th antenna of the radar transmitter transmits a single-tone signal, i.e.,

$$s_{hm}(i) = e^{\mathrm{j}2\pi i k_{hm} \Delta}, \ i = 0, 1, \cdots, L-1, \tag{3}$$

where i the sample index, $L = \lfloor T/T_\mathrm{s} \rceil$ is the number of samples per hop and T_s is the sampling interval. Here, $\lfloor \cdot \rceil$ rounds to the closest integer, and as in (2), Δ is a positive integer. Since k_{hm} is also an integer, the real and imaginary parts of $s_{hm}(i)$ $(\forall h, m)$ consist of integer multiples of cycles. Exemplary $s_{hm}(i)$'s are provided in Node A of Fig. 3. It is known that two sinusoidal signals are orthogonal if they have integer multiples of cycles and different frequencies. This can be readily validated by $\sum_{i=0}^{L-1} s_{hm}^*(i) s_{hm'}(i) = 0$, where $(\cdot)^*$ takes the complex conjugate.

Before $s_{hm}(i)$ is transmitted from radar antenna m, F_{hm} is multiplied onto the signal to embed communication information; if not required, we can simply take $F_{hm} = 1$. Propagating from the radar transmitter to the communication receiver through the flat-fading SV channel illustrated in Section II-A, the M signals are scaled by the channel coefficients which are the elements of the vector $\mathbf{b}$ given in (1). The scaling is illustrated in Fig. 3 through the second column of multipliers before Node B. The signal received by the single-antenna communication receiver is the sum of the scaled signals plus an AWGN (inherent in any receiver). An AWGN is also exemplified in Fig. 3. Based on the above description, the baseband signal at the communication receiver, i.e., the signal arriving at Node B, is given by

$$\begin{aligned} &y_h(i) = \mathbf{b}^\mathrm{H} \mathbf{s}_h(i) + \xi_h(i), \\ &\text{s.t. } \mathbf{s}_h(i) = [s_{h0}(i) F_{h0}(i), \cdots, s_{h(M-1)}(i) F_{h(M-1)}(i)]^\mathrm{T}, \end{aligned} \tag{4}$$

where $\mathbf{b}$ is the channel vector given in (1), $(\cdot)^\mathrm{H}$ denotes the conjugate transpose, $\mathbf{s}_h(i)$ collected the information-modulated radar signals transmitted by M antennas, and $\xi_h(i)$ is an AWGN. Note that the above signal model is obtained based on a perfect timing, which may be challenging to realize in practice, as will be discussed in Section III-B. Differentiated by F_{hm}, we have different signaling schemes/strategies which are illustrated next.

III. Overview of Existing Signaling Strategies for FH-MIMO DFRC

Several signaling strategies have been specifically designed for FH-MIMO DFRC. Overall, they can be categorized into two groups, one based on conventional phase modulations [10]–[13] and the other exploiting the diversity in frequency hopping [14]. In this section, the existing signaling strategies are first reviewed with their modulation and demodulation processing illustrated. Then the strategies are compared from various aspects.

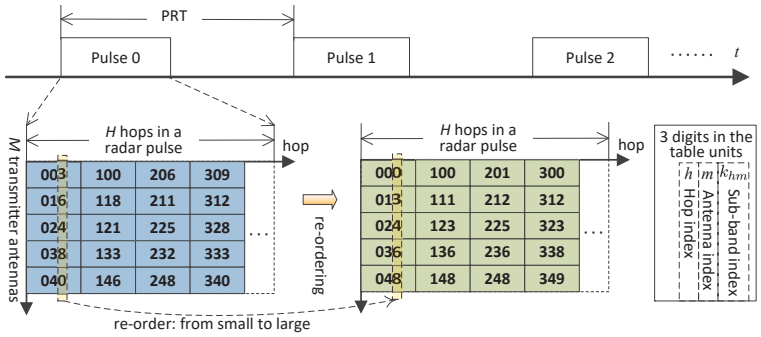

Fig. 2: Illustration of the signal structure of an FH-MIMO radar, where each radar pulse is divided into H hops, each hop randomly selects M (out of K in total) sub-bands as hopping frequencies, one for each antenna. The conventional FH-MIMO waveform can have non-ordered sub-bands assigned over antennas in each hop, as seen from the waveform block shown on the left. A re-ordering process can be introduced to re-arrange the sub-bands in each hop in a deterministic order, such as from small to large in the figure.

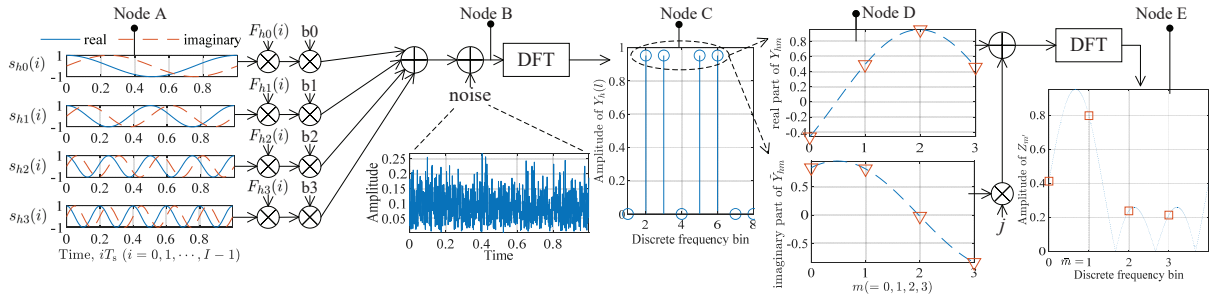

Fig. 3: Illustration of the signal flow in FH-MIMO DFRC. For ease of illustration yet without loss of generality, four antennas, i.e., $M = 4$ are considered. At hop h (whose value does not affect the signal flow and hence is not specified), the sub-bands $1, 2, 4$ and 5 are selected for antennas $0, 1, 2$ and 3, respectively, which leads to $k_{h0} = 1$, $k_{h1} = 2$, $k_{h2} = 4$ and $k_{h3} = 5$. Here k_{hm} $(m = 0, 1, 2, 3)$ is the sub-band index illustrated in Fig. 2. Nodes A, B, C, D and E illustrate the signals given in (3), (4), (5), (6) and (7), respectively. The detailed descriptions between the nodes and equations are presented in the respective contexts of the equations.

A. Information Modulation

1) Phase Modulations: In [10], [11], PSK is introduced to FH-MIMO DFRC by embedding PSK phases into radar signals. More specifically, a constant phase $F_{hm} = e^{\mathrm{j}\varpi_{hm}}$ is taken in (4), where $\varpi_{hm} \in \Omega_J$ $(J \geq 1)$ and $\Omega_J = \left\{0, \cdots, \frac{2\pi(2^J-1)}{2^J}\right\}$ is the J-bit PSK constellation. In [12], the differential PSK (DPSK) is proposed to replace PSK, so as to reduce range sidelobes and out-of-band transmission. To further improve the spectral shape of the modulated radar signal, the continuous phase modulation (CPM) is introduced in FH-MIMO DFRC [13]. The underlying principle is that signals with smoother modulating phase correspond to lower out-of-band transmission.

2) Frequency Hopping-based Modulation: In [14], the combinations of hopping frequencies are used to convey information bits, referred to as frequency hopping code selection (FHCS). As illustrated earlier, only M out of K sub-bands are selected each hop as hopping frequencies. Thus, there are C_K^M combinations of hopping frequencies, and the combinations can be employed to convey up to $\lfloor \log_2 C_K^M \rfloor$ number of information bits per radar hop, where $\lfloor \cdot \rfloor$ rounds towards negative infinity.

3) Comparing Two Modulation Methods and Discussions: Both modulation methods will somewhat change the original FH-MIMO radar system, but in a different manner. The phase modulations change the phases of radar signals, and the phases can severely vary over antennas and hops depending on the information bits to be sent. In contrast, FHCS leaves the phases unaltered but changes the hopping frequencies over hops. A benefit of the phase modulation is that it can suppress the periodic spikes in the sidelobe regions of the range ambiguity function, as will be seen shortly. This benefit is not shared by FHCS-modulated waveform which has similar range ambiguity function to the original radar waveform, since both waveforms are essentially based on randomly selected hopping frequencies. However, a prominent advantage of FHCS over phase modulations is the reduced complexity in information demodulation and the improved robustness against channel estimation errors, as will be detailed in Section III-B.

Fig. 4 compares the range ambiguity functions of an FH-MIMO radar under different modulations. The range ambiguity function is the zero-Doppler cut of the ambiguity function, and hence is in essence the autocorrelation function [9]. Following the related work [9]–[13], we use the term "range ambiguity function" in this article. From Fig. 4, we see the aforementioned spikes in both the original radar waveform and the FHCS-modulated one. These spikes are caused by the re-use of sub-bands as hopping frequencies over hops; refer to [10] for an in-depth analysis. We also see from Fig. 4 that the sidelobe spikes are suppressed by the binary PSK (BPSK) modulation. This is because BPSK scrambles the phases of the original radar waveform over hops and antennas, hence preventing the coherent accumulation in the sidelobe regions of the range ambiguity function. To this end, it is recommended to jointly use FHCS and PSK in FH-MIMO

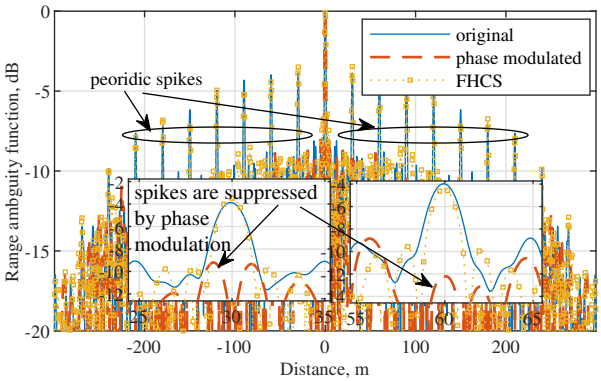

Fig. 4: Comparing the range ambiguity functions of an FH-MIMO radar under different information modulations, where BPSK is used for the phase modulated waveform and the simulation parameters are given in Table I. For smoother results, $T_{\rm s} = 1/(10B)$ is used here. As illustrated in the zoomed-in sub-figures, phase modulation suppresses the sidelobe spikes. For better clarity, we only show the suppression of two spikes, while the suppression is effective for all the spikes.

DFRC, as designed in [17].

B. Information Demodulation

We proceed to describe the methods that demodulate the information embedded in radar signals. As seen from Node B in Fig. 3, the signals transmitted by different antennas of the radar transmitter are superimposed at a communication receiver. Nevertheless, based on the waveform orthogonality enforced by (2) and validated by Node A in Fig. 3, the signals can be separated in the frequency domain. The L-dimensional discrete Fourier transform (DFT) of $y_h(i)$ yields

$$Y_h(l) = \beta_0 e^{-\mathrm{j}mu_0} e^{\mathrm{j}\varpi_{hm}} \delta(l - l^*_{hm}),\ l^*_{hm} = k_{hm}\Delta, \qquad (5)$$

where $P = 1$ is taken as in prior works [10]–[16] and $\delta(l)$ is the Dirac delta function. The noise term is dropped for illustration convenience. The amplitude of the above DFT result is demonstrated in Node C of Fig. 3. In the figure, $k_{h0} = 1$, $k_{h1} = 2$, $k_{h2} = 4$, $k_{h3} = 5$ and $\Delta = 1$ are set, which leads to $l^*_{hm} = 1, 2, 4$ and 5 for $m = 0, 1, 2$ and 3, respectively. In Node C of Fig. 3, we see that there are four separated peaks at the 2nd, 3rd, 5th and 6th discrete bins. Note that l^*_{hm} starts from zero while the bin index from one.

1) FHCS Demodulation: Based on $Y_h(l)$, an FHCS symbol can be readily demodulated by identifying the peaks in the magnitude of $Y_h(l)$. The indexes of the peaks result in the estimated set of $\{l^*_{hm}\ \forall m\}$. Based on the relation between l^*_{hm} and k_{hm} given in (5), we can obtain the combination of hopping frequencies used in the radar hop. The estimated combination is then used to demodulate the FHCS symbol.

2) PSK Demodulation: Provided that k_{hm} is known by the UE, l^*_{hm} is then obtained based on (5). Extract the value of $Y_h(l)$ at $l = l^*_{hm}$, leading to

$$\tilde{Y}_{hm} = Y_h(l^*_{hm}) = \beta_0 e^{-\mathrm{j}mu_0} e^{\mathrm{j}\varpi_{hm}}. \qquad (6)$$

Note that these extracted signals are exemplified by the peaks in Node C of Fig. 3. Their real and imaginary parts are plotted in Node D in the figure. In the figure, $\varpi_{hm} = 0$ $(\forall h, m)$ is taken for illustration clarity. Thus, the real and imaginary parts are samples of cosine and sine functions with the angular frequency of u_0 and initial phase of $\angle\beta_0$. Here, $\angle(\cdot)$ takes the angle of a complex number. In the communication receiver, ϖ_{hm} needs to be estimated for information demodulation. To do so, $\beta_0 e^{-\mathrm{j}mu_0}$ needs to be suppressed first.

3) Discussions: From the above description, the following information ($\mathcal{I}1$)-($\mathcal{I}3$) are necessary for demodulating information symbols in FH-MIMO DFRC:

($\mathcal{I}1$) Accurate timing;
($\mathcal{I}2$) k_{hm} — the hopping frequency used by antenna m at hop h, as illustrated in Fig. 2; and
($\mathcal{I}3$) $\beta_0 e^{-\mathrm{j}mu_0}$ — the channel response, as shown in Fig. 1.

Note that ($\mathcal{I}1$) is applied to obtain (5) from (4) so that inter-hop and inter-antenna interferences are avoided. To this end, both FHCS and PSK demodulations implicitly apply ($\mathcal{I}1$), since the demodulations are performed based on (5). As for ($\mathcal{I}2$) and ($\mathcal{I}3$), they are not required for FHCS demodulation and are explicitly used in the PSK demodulation.

In practice, none of the information ($\mathcal{I}1$)-($\mathcal{I}3$) is easy to acquire. For the first two information ($\mathcal{I}1$) and ($\mathcal{I}2$), a specific synchronization link may be required to establish between the radar and UE. Such a link can make the radar require extra resources, e.g., hardware and frequency etc. More specifically, an extra antenna and correspondingly RF chain can be required for synchronization, since the existing antennas of the radar transmitter are fully occupied for radar detection. Besides, a different frequency band (from the original radar operating frequency) can be required to establish the synchronization link so as to reduce the mutual interference between radar and communications. The acquisition of the third information ($\mathcal{I}3$) is subject to that of the first two, since inter-antenna and inter-hop interference will be incurred without an accurate timing.

C. Comparing Signaling Schemes for FH-MIMO DFRC

The aforementioned signaling schemes are compared in terms of their impact on radar performance, their communication performance and the necessary information for demodulation. The comparison is summarized in Table II. Note that the radar ambiguity functions and spectral containment of the signaling schemes have been comprehensively compared in [15]. The data rates of different schemes are provided in the works [10]–[14]. Yet, the necessary information is overlooked in most existing works which consider ideally known ($\mathcal{I}1$)-($\mathcal{I}3$).

We notice that DPSK demodulation does not require ($\mathcal{I}2$) in quasi-static channels, since the channel response is suppressed in the differential processing [12]. In contrast to phase modulation-based schemes, FHCS does not require ($\mathcal{I}2$) or ($\mathcal{I}3$), since it pursues to estimate ($\mathcal{I}2$) from the magnitude of the frequency-domain signal, as illustrated in Section III-B1. Strictly speaking, FHCS can be demodulated without requiring ($\mathcal{I}1$), provided that the timing offset is small. However, inter-hop and inter-antenna interferences are introduced given a non-zero timing offset, which consequently degrades the demodulation performance of FHCS. As will be shown in Section IV-C, the demodulation performance of FHCS has a significant impact on that of PSK. To this end, accurate timing is still

TABLE II: Comparing Existing Signaling Schemes for FH-MIMO DFRC.

Modulation	PSK [11]	DPSK [12]	CPM [13]	FHCS [14]
Data Rate	PRF$\times HMJ$	PRF$\times HMJ$	PRF$\times HM\log_2 M$	PRF$\times H\lfloor\log_2 C_K^M\rfloor$
Range Sidelobe	low	lower	lowest	high with periodic spikes
Spectral Containment	good	better	best	poor
Necessary Information for Demodulation	($\mathcal{I}1$), ($\mathcal{I}2$) and ($\mathcal{I}3$)	($\mathcal{I}1$) and ($\mathcal{I}2$)	($\mathcal{I}1$), ($\mathcal{I}2$) and ($\mathcal{I}3$)	($\mathcal{I}1$) (not strictly necessary)

Notes: J is the PSK modulation order. For instance, $J = 1, 2$ and 3 denotes BPSK, QPSK and 8-PSK, respectively.

TABLE I: Parameter Definitions and Settings for Simulations and Illustrations Throughout the Article (Unless Otherwise Specifed)

Variable	Value	Definitions
H	10	number of hops per radar pulse
M	10	number of antennas at radar transmitter
B	100 MHz	radar bandwidth
K	20	number of sub-bands
T	0.2μs	time duration of a hop
$T_{\rm s}$	$1/(2B)$	sampling time
Δ	1	BT/K
τ	0.2	duty cycle of a radar pulse

desired for FHCS to attain a high communication performance of FH-MIMO DFRC.

We also notice that, unlike the phase modulation schemes having monotonically increasing data rates with respect to (w.r.t.) M, the data rate of FHCS first increases with M, then plateaus as M reaches $K/2$, and starts decreasing as M keeps increasing, due to the binomial coefficient in its rate expression. To improve the data rate, FHCS can be employed in combination with the phase modulation schemes, as developed in [16], [17]. However, the cost of the rate improvement is that more necessary information, i.e., ($\mathcal{I}_2$) and ($\mathcal{I}_3$), will be required for demodulation. This leads to the trade-off between data rate and demodulation performance in FH-MIMO DFRC.

As for the demodulation performance of different singling schemes developed for FH-MIMO DFRC, no analytical result has been published yet. In conventional communications, the asymptotic symbol error rate (SER) of DPSK and CPM is generally inferior to that of PSK, particularly when the modulation order is high; and the optimal receiver of CPM can be more difficult to achieve compared with the other two phase modulations [21]. These general results, however, may not hold for FH-MIMO DFRC, since the phase demodulation performance is subject to the quality of ($\mathcal{I}2$) acquired in practice. As will be validated in Section IV-C, this coupling will significantly affect the demodulation performance of PSK.

IV. Channel Estimation for FH-MIMO DFRC

As illustrated above, most existing signaling schemes for FH-MIMO DFRC require accurate channel information to perform demodulation. Yet, to the best of our knowledge, only a few published work [16], [17] develop channel estimation scheme for FH-MIMO DFRC. In this section, we first review the channel estimation methods designed for DFRC (not necessarily based on FH-MIMO radar), and then briefly introduce the solution developed in [16].

A. Overview of Channel Estimations in DFRC

To the best of our knowledge, few published works have explicitly dealt with the channel estimation issue of DFRC. Specifically, sparse recovery-based channel estimation methods are developed in [22], [23] which coordinate radar and communication receiver using probing beams. In a different yet relevant context (spectrum sharing), interference channel between radar and communication is estimated to achieve co-existence; refer to [4] for a review on those methods. In some recent DFRC works [3], [4] channel estimation methods are developed, which, however, are based on new (future) DFRC waveforms/platforms. These new designs are specifically tailored for dual functions and are non-trivial to be applied in FH-MIMO DFRC. A common feature captured by most of the above methods is the full cooperation between radar and communication. In contrast, the channel estimation for FH-MIMO DFRC is likely to be carried out at a low-profile communication receiver with low computing power and a small number of (or a single) antennas.

B. Recent Advances in Channel Estimation for FH-MIMO DFRC

In [16], a channel estimation scheme is developed for FH-MIMO DFRC to estimate the hopping frequencies and channel parameters, assuming an accurate timing.

1) Estimating Hopping Frequency: A novel FH-MIMO waveform with minor revisions to the conventional one is designed in [16], which enables UE to estimate k_{hm}, i.e., the hopping frequency used by the m-th radar transmitter at any hop h. In particular, it is proposed that:"*the radar first randomly selects available sub-bands as hopping frequencies, as it usually does, then re-orders the frequencies in a deterministic order, ascending for instance, before assigning to each transmitter antenna.*" The waveform re-ordering is illustrated in Fig. 2. This simple processing enables k_{hm} to be estimated at the UE (instead of being acquired from the radar).

According to the novel waveform illustrated above, $k_{hm} < k_{hm'}$ $(\forall m, m', m < m')$ is ensured, where m and m' are indexes of different antennas. Taking the first column of the re-ordered waveform in Fig. 2 for an example, we see that $k_{00} = 0$, $k_{01} = 3$, $k_{02} = 4$, $k_{03} = 6$ and $k_{04} = 8$, which satisfies the above inequality. This relation, applied in the set of sub-band indexes obtained in (5), leads to an estimate of k_{hm} $\forall m$. Importantly, it is also proved in [16] that the above re-ordering does not incur any change to the range ambiguity function of the FH-MIMO radar.

2) Estimating Channel Response: To perform channel estimation, the first hop at each pulse is designated for channel

estimation [16] and hence has no information embedding, i.e., $\varpi_{0m} = 0\ \forall m$. Next, $\tilde{Y}_{0m} = \beta_0 e^{-\mathrm{j}mu_0}$, as given in (6), are used for estimating u_0 and β_0. The path AoA u_0 can be regarded as a discrete frequency of a single-tone signal, which has been demonstrated in Node D of Fig. 3. Taking the DFT of $\tilde{Y}_{0m}$ (over m), we obtain

$$Z_{m'} = \sum_{m=0}^{M-1} \tilde{Y}_{0m} e^{-j\frac{2\pi m m'}{M}},\ m' = 0, 1, \cdots, M-1, \quad (7)$$

which is illustrated in Node E of Fig. 3. We see that the DFT result on the second discrete frequency bin, denoted by $\tilde{m}$, has the maximum amplitude. This indicates that the true u_0 is closer to $2\pi\tilde{m}/M$ compared with $2\pi m/M$ for $\forall m(=0,1,2,3)$ and $m \neq \tilde{m}$. To improve the u_0 estimation, interpolating DFT coefficients has been suggested in [24], [25]. For completeness of the article, we simply summarize the steps for u_0 estimation based on the q-shift estimator (QSE), originally designed in [24] and later improved in [25]. The technical details are suppressed here (interested readers are referred to [24], [25]).

To refine the estimate of u_0, QSE interpolates the DFT coefficients around $\tilde{m}$, yielding $Z_{\pm} = \sum_{m=0}^{M-1} \tilde{Y}_{0m} e^{-j\frac{2\pi m(\tilde{m}+\zeta\pm\epsilon)}{M}}$, where ζ is an interpolation factor to be updated iteratively and ϵ is an intermediate variable satisfying $\epsilon \leq \min\{M^{-\frac{1}{3}}, 0.32\}$ [25, Eq. (23)]. Construct a ratio based on $Z_{\pm}$, as given by $\gamma = \frac{Z_+ - Z_-}{Z_+ + Z_-}$. Use the ratio γ to update ζ by the relation: $\zeta = \frac{\epsilon \cos^2(\pi\epsilon)}{1 - \pi\epsilon\cot(\pi\epsilon)} \times \Re\{\gamma\} + \zeta$, where ζ on the right-hand side (RHS) of the equality is the old value, and $\Re\{\cdot\}$ takes the real part of a complex number. By updating ζ for three times, the algorithm can generally converge [24]. The final estimate of u_0 and β_0 can be given by $\hat{u}_0 = \frac{2\pi}{M}(\tilde{m} + \zeta)$ and $\hat{\beta}_0 = \frac{1}{M}\sum_{m=0}^{M-1} \tilde{Y}_{0m} e^{jm\hat{u}_0}$.

C. Performance Illustration

Numerical results are provided here to demonstrate the high estimation performance of the method elaborated on above. Fig. 5 plots the mean squared error (MSE) of the estimated channel parameters against the SNR, as measured based on (4) and denoted by γ_0 below. To evaluate the MSE of $\hat{u}_0$, $N = 2 \times 10^4$ independent trials are performed, and the MSE is calculated by $\sum_{n=0}^{N-1}(\hat{u}_0(n) - u_0)^2/N$, where $\hat{u}_0(n)$ is an estimate of u_0 and is obtained in the n-th independent trial. The MSE of $\hat{\beta}_0$ is calculated similarly. Based on [24], the Cramér-Rao lower bound (CRLB) of u_0 estimation is given by $3/(\pi^2 ML\gamma_0)$.

We see from Fig. 5 that the MSEs of both $\hat{u}_0$ and $\hat{\beta}_0$ monotonically decrease with the SNR. In particular, the MSE of $\hat{u}_0$ approaches the CRLB when the SNR exceeds 6 dB, which validates the high accuracy of the estimation method provided in Section IV-B2. A noticeable gap exists between the MSE of $\hat{u}_0$ and the CRLB. This is caused by the threshold effect when detecting the DFT peak for a coarse u_0 estimate. Interested readers may refer to [24] for more details on this effect.

Fig. 6 plots the SER of BPSK and FHCS-based FH-MIMO DFRC, where the channel estimates obtained at the estimation

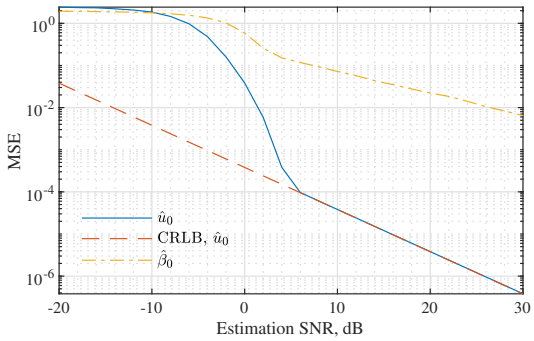

Fig. 5: Illustration of the channel estimation performance using the method elaborated on in Section IV-B. The AoD of the LoS path is set as $u_0 = \pi/2$; the path gain β_0 has unit amplitude but random angles uniformly taken in $[0, 2\pi]$ radius; refer to Table I for other parameter settings.

SNR of 10 dB are used to perform information demodulations. The x-axis of the figure is based on the energy per bit to noise power density ratio, which is calculated by $LM\gamma_0 BT/\tilde{J}$, where $\tilde{J}$ is the number of bits conveyed per radar hop. Specifically, $\tilde{J} = M = 10$ for BPSK, $\tilde{J} = \lfloor \log_2 C_K^M \rfloor = 17$ for FHCS, and $\tilde{J} = 10+17 = 27$ for the combination of FHCS and BPSK. Given the parameters in Table. I, each radar pulse is able to transmit $\tilde{J} \times H = 27 \times 10 = 270$ (bits). The pulse repetition time of the radar is given by $T \times H/\tau = 10\mu$s, where τ is the duty cycle of the radar (i.e., the fraction of the time that the radar transmitter is active). Thus, the data rate is calculated as

$$\tilde{J} \times H/(TH/\tau) = 270/10 \times 10^6 = 27\ \text{(Mbps)}. \quad (8)$$

We see from Fig. 6 that, with either the estimated k_{hm} or its true value, the SER performance of BPSK achieved based on the estimated channel parameters approaches the performance under the ideally known channels. This validates the high accuracy of the channel estimation method. We also see from the figure that, employing the estimated channel parameters, FHCS outperforms BPSK w.r.t the SER against $\mathrm{E_b/N_0}$, which owes to the improved data rate of FHCS over BPSK. Since the combination of FHCS and BPSK further improves the data rate, the SER performance of the combination is improved over those of the individual modulations.

We further see from Fig. 6 that the k_{hm} has a much stronger impact on the SER of BPSK compared with the channel parameters β_0 and u_0. To achieve the SER of 10^{-4}, using the true value of k_{hm} can reduce the required $\mathrm{E_b/N_0}$ by 5 dB, compared with using the estimated k_{hm}. On one hand, this observation indicates that the final SER performance of FH-MIMO DFRC should be carefully analyzed after taking the detection performance of k_{hm} into account, as discussed in Section III-C. On the other hand, this observation suggests that new methods should be developed to improve the estimation performance of k_{hm}.

V. Major Research Challenges in FH-MIMO DFRC

As a newly conceived DFRC architecture based on FH-MIMO radar, there are still many challenging issues to be addressed effectively. In this section, we discuss the major challenges and suggest potential solutions for future research.

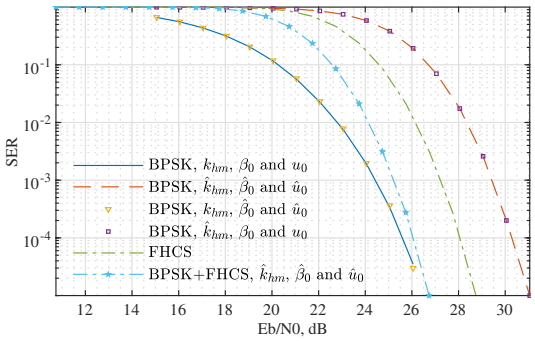

Fig. 6: Illustration of the SER performance of FH-MIMO DFRC under different modulations, where $\hat{k}_{hm}$ is the estimated hopping frequency used by antenna m at hop h; $\hat{\beta}_0$ and $\hat{u}_0$ are obtained at the estimation SNR of 10 dB; and k_{hm}, β_0 and u_0 are the true values. Other parameters are given in Table I. The FHCS demodulation is performed by estimating k_{hm}, which is independent on β_0 and u_0. The BPSK demodulation relies on k_{hm}, β_0 and u_0, which is explicitly shown in the legend. When the accent symbol is added, e.g., $\hat{(\cdot)}$, the estimate of a variable is used for demodulation.

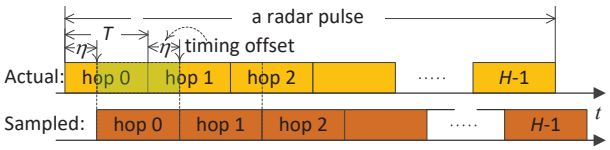

Fig. 7: Illustration of the impact of a non-zero timing offset on the signal sampling at a UE.

A. New Signaling Strategies Enabling Higher Data Rates

As shown in (8), the overall data rate achieved by FH-MIMO DFRC is 27 Mbps, under the condition that BPSK and FHCS is combined, the radar has 10 antennas and a bandwidth of 100 MHz, and the UE has a single antenna. To provide an effective high-speed G2A communication link using FH-MIMO DFRC, new signaling strategies are required.

We remark that the information conveyed in the hopping frequencies has not been fully explored yet. In light of FHCS as illustrated in Section III-A, the permutations of hopping frequencies can be employed to convey information bits [18]. Using permutations is expected to increase the data rate dramatically, since the number of permutations can be huge. Take the parameters used in Fig. 6 for an example. The number of permutations that permutes $M(=10)$ out of $K(=20)$ sub-bands can be larger than 670 billion, which, in theory, is able to convey up to 39 bits per radar hop. Similar to the rate calculation given in (8), the data rate achieved by using permutations can be given by $39\times10/10\times10^6 = 39$ Mbps. As a result, an increase of $12(=39-27)$ Mbps in data rate can be achieved through using permutations. This improvement of data rate, however, requires a proper demodulation method to be developed at the UE. One challenge is to deal with the reduced Euclidean distances between the permutations. Another challenge is to develop effective receiving schemes for UE to reliably demodulate the permutation-based information symbol, particularly when the issues discussed sequentially are present.

B. Timing Offset

The prior works on FH-MIMO DFRC [10]–[16] assume perfect timing which is also the case in our elaboration provided in Section IV. However, there can be a non-zero timing offset in practice, particularly when a synchronization link between the radar and the UE is unavailable; see Section III-B for details. In a packet-based communication, the UE can attain a coarse timing by performing conventional methods like energy or correlation-based detection [17]. Provided a non-zero timing offset, a sampled hop spans over two actual hops, as illustrated in Fig. 7. As a consequence, there will be inter-hop interference introduced to the received signals. Moreover, due to the incomplete sampling of a hop, the waveform orthogonality of the FH-MIMO radar, as ensured by the integer multiple of cycles of different sinusoidal signals in each hop (see Node A of Fig. 3), is destroyed, hence introducing inter-antenna interference [17].

It is noteworthy that the impact of timing offset is frequency-varying, which can result in great difficulty for channel estimation and information demodulation. Based on the baseband radar signal given in (3), we can model the received signal with a non-zero timing offset, as given by $e^{\mathrm{j}2\pi(i-L_\eta)k_{hm}\Delta}$, where L_η is the number of samples in the non-zero timing offset denoted by η. Since k_{hm} varies across hop h and antenna m, the phase nuisance incurred by L_η also varies over hops and antennas.

A seemingly straightforward solution to this issue is to perform additional timing offset estimation, which helps recover a complete hop and revive the methods for channel estimation illustrated in Section IV. However, the estimation of the timing offset is challenging. As mentioned earlier, inter-antenna and inter-hop interference exists for any given non-zero timing offset. On the other hand, the antenna- and hop-varying phase resulted from the timing offset is coupled with the phase of channel response in a point-wise manner. This makes the estimation of either part challenging.

To address the above challenges, we may resort to the DoF available in the FH-MIMO radar waveform. For example, if $k_{hm} = 0$, then the phase caused by the timing offset is removed according to $e^{\mathrm{j}2\pi(i-L_\eta)k_{hm}\Delta}$. Note that, in any hop h, only one k_{hm} $(\forall m = 0, 1, \cdots, M-1)$ can take zero, so as to comply with the waveform orthogonality constraint of an FH-MIMO radar, as given in (2). Moreover, the specific values of h and m, need to be designed in the development of the methods for estimating the timing offset and communication channel.

C. Multi-Path Channel

Thus far, only the LoS-dominated AWGN channel is considered for FH-MIMO DFRC. As discussed in Section II-A, it can be practical to consider the LoS channel for some scenarios, such as the G2A communications between a ground-based radar and an high-altitude platform; see Fig. 1. However, as also illustrated in the figure, multi-path fading can happen in FH-MIMO DFRC, when the airborne UE, e.g., UAV, flies at a low altitude. Under multi-path fading, the signal can be severely attenuated, when arriving at the receiver.

Fig. 8 illustrates the signal attenuation caused by multi-path fading by plotting $|Y_h(l)|$, namely, the magnitude of the DFT of the UE-received signal within a radar hop, where $Y_h(l)$ is

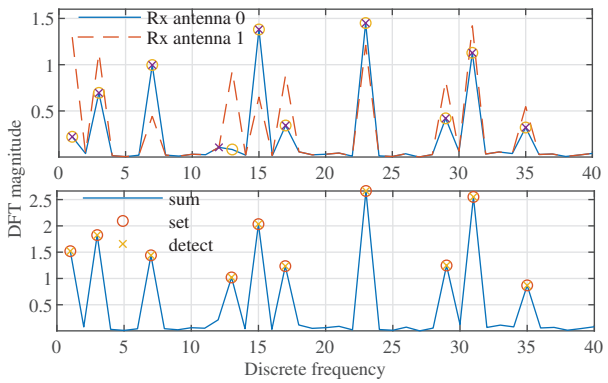

Fig. 8: Illustration of the severe signal attenuation caused by multi-path fading, where the Rician channel is considered with the Rician factor of 5 dB and the LoS path takes the unit power. Two receiver (Rx) antennas with the spacing of half a wavelength are considered at the UE, each with an independent AWGN of -10 dB noise power. The radar parameters are set according to Table I.

given in (5) and an accurate timing is assumed here. Based on the waveform design illustrated in Section IV-B1, the m-th DFT peak corresponds to the signal from transmitter (Tx) antenna m $(m = 0, 1, \cdots, M-1)$ at the radar. We see from the figure that a severe attenuation of the signal transmitted by Tx antenna three is observed on the first receiver (Rx) antenna at the UE. Performing the method elaborated in Section IV-B1 to detect the hopping frequency, we see from the upper sub-figure in Fig. 8 that the hopping frequency of the fourth antenna is incorrectly detected. This incorrect detection will lead to the incorrect demodulation of not only hopping frequency-based modulations, e.g., FHCS, but also phase-based modulations, e.g., PSK. For the later modulation, the signal used for demodulation is extracted based on the identified indexes of the DFT peaks (that are used for FHCS demodulation).

A viable solution to combating the multi-path fading in FH-MIMO DFRC is equipping the UE with multiple Rx antennas and exploiting the antenna diversity. This is demonstrated in Fig. 8. The upper sub-figure also plots the magnitude of the DFT of the signal received by a different Rx antenna. Clearly, the attenuation caused by multi-path fading to the signal transmitted by the fourth antenna is greatly relieved. By combining the signals of the two antennas incoherently, the sum signal can be used to detect the hopping frequency more reliably; see the right sub-figure in Fig. 8. It is worth mentioning that improving the detecting performance of the hopping frequencies also substantially benefits to the SER performance of demodulating phase-based modulations, as demonstrated in Fig. 6. With the benefits of using multi-antenna receivers at the UE recognized, we should also bear in mind that effective signal reception also relies on the accurate estimation of timing offset and channel parameters. These practical issues have not been properly addressed for a single-antenna receiver yet, not to mention multi-antenna configurations.

D. Security Issues

MIMO radar-based DFRC can have a security issue, as underlined in some recent studies [26]. The security issue can affect the FH-MIMO DFRC as well, since the underlying FH-MIMO radar has an omnidirectional radiation pattern given omnidirectional antenna elements [18]. To this end, provided that the signal framework used between the radar and the legitimate UE is known by an eavesdropper, the radar-transmitted signal can be demodulated by an eavesdropper using the method provided in Section IV. Here, we consider the situation where the conventional secret key-based encryption either fails or is not performed. It is not impossible for the secret key-based encryption to be "cracked" with the fast developments and advances in computing power devices [27]. Moreover, secret key-based encryption may not always be preferable, particularly for applications that are delay-sensitive, power-limited, and processing-restricted [27].

As an effective supplement to upper-layer security techniques, physical layer security has attracted increasing attention recently in 5G and beyond communications, and can be a promising solution to achieving a secure FH-MIMO DFRC. Specifically, the secrecy enhancement method developed in [28] may be tailored for FH-MIMO DFRC. In short, the method randomly selects a subset of (at least two) antennas in a transmitter array and half of the antennas in the subset multiply their beamforming weights by -1. Note that the larger the number of antennas in the subset, the greater secrecy enhancement can be achieved, which, however, leads to smaller communication data rates. Through the above processing, AWGNs are injected to the whole spatial region except for the direction of a targeted receiver. The method may be tailored for FH-MIMO DFRC, however, at the cost of reducing the data rate. This is a typical trade off between the secrecy rate and data rate of a communication system. To this end, the security issue can be treated in combination with designing new signaling strategies for high data rates, as discussed in Section V-A.

E. Real-life Demonstration of FH-MIMO DFRC

Last but not the least, it is worth pointing out that real-life measurements and demonstrations of FH-MIMO DFRC have not been reported yet in the open literature. This calls for interested researchers in both radar and communication fields to carry out such experiments. On the other hand, we notice from the literature, e.g., [29], [30], that the software-defined radio (SDR) platforms are often used for validating MIMO radar waveforms (not FH-MIMO though). As a cost- and time-efficient method, and it may be convenient to use SDR platforms to validate FH-MIMO DFRC as well. In particular, there are two popular SDR platforms. The open-source GNURadio, e.g., ETTUS X310, can support 6 GHz carrier frequency and up to 120 MHz bandwidth [29]. A more powerful SDR platform is developed by the Ohio State University (OSU), which supports up to 500 MHz instantaneous bandwidth and a center frequency tunable in 2 to 18 GHz [30]. Either X310 or OSU-SDR only supports two transmitter and two receiver chains per platform. Thus, we may need to jointly use several SDRs to allow more transceivers in practice.

VI. Conclusions

In this article, a comprehensive review on FH-MIMO DFRC is provided. The potential applications and channel scenarios are presented. The existing signaling strategies for FH-MIMO DFRC are surveyed with their performance compared from various aspects. A channel estimation scheme specifically designed for FH-MIMO DFRC is presented with numerical results to demonstrate estimation and communication performance. Major issues remaining in FH-MIMO DFRC are discussed with potential solutions suggested. We envision that with the highlighted challenges properly addressed in the future, FH-MIMO DFRC is poised to become a viable solution to long-range radar and communications, and forthcoming ISTN and 6G mobile networks.

References

[1] X. You *et al.*, "Towards 6G wireless communication networks: Vision, enabling technologies, and new paradigm shifts," *Science China Information Sciences*, vol. 64, no. 1, pp. 1–74, 2021.

[2] L. Zheng, M. Lops, Y. C. Eldar, and X. Wang, "Radar and communication coexistence: An overview: A review of recent methods," *IEEE Signal Process. Mag.*, vol. 36, no. 5, pp. 85–99, 2019.

[3] M. L. Rahman, J. A. Zhang, K. Wu, X. Huang, Y. J. Guo, S. Chen, and J. Yuan, "Enabling joint communication and radio sensing in mobile networks–a survey," *arXiv preprint arXiv:2006.07559*, 2020.

[4] F. Liu *et al.*, "Joint radar and communication design: Applications, state-of-the-art, and the road ahead," *IEEE Trans. Commun.*, vol. 68, no. 6, pp. 3834–3862, 2020.

[5] A. Hassanien, M. G. Amin, E. Aboutanios, and B. Himed, "Dual-function radar communication systems: A solution to the spectrum congestion problem," *IEEE Signal Process. Mag.*, vol. 36, no. 5, pp. 115–126, Sep. 2019.

[6] S. C. Surender and R. M. Narayanan, "UWB noise-OFDM netted radar: Physical layer design and analysis," *IEEE Trans. Aerosp. Electron. Syst.*, vol. 47, no. 2, pp. 1380–1400, 2011.

[7] P. Kumari, S. A. Vorobyov, and R. W. Heath, "Adaptive virtual waveform design for millimeter-wave joint communication-radar," *IEEE Trans. Signal Process.*, pp. 1–1, 2019.

[8] A. Hassanien, M. G. Amin, Y. D. Zhang, and F. Ahmad, "Signaling strategies for dual-function radar communications: an overview," *IEEE Aerosp. Electron. Syst. Mag.*, vol. 31, no. 10, pp. 36–45, 2016.

[9] C. Chen and P. P. Vaidyanathan, "MIMO radar ambiguity properties and optimization using frequency-hopping waveforms," *IEEE Trans. Signal Process.*, vol. 56, no. 12, pp. 5926–5936, Dec 2008.

[10] I. P. Eedara *et al.*, "Ambiguity function analysis for dual-function radar communications using PSK signaling," in *52nd Asilomar Conf. Signals, Syst., and Computers*, Oct 2018, pp. 900–904.

[11] I. P. Eedara, M. G. Amin, and A. Hassanien, "Analysis of communication symbol embedding in FH MIMO radar platforms," in *2019 IEEE Radar Conf. (RadarConf)*, April 2019, pp. 1–6.

[12] I. P. Eedara and M. G. Amin, "Dual function FH MIMO radar system with DPSK signal embedding," in *2019 27th European Signal Process. Conf. (EUSIPCO)*, Sep. 2019, pp. 1–5.

[13] I. P. Eedara, M. G. Amin, and A. Hassanien, "Controlling clutter modulation in frequency hopping MIMO dual-function radar communication systems," in *IEEE International Radar Conf.*, 2020, pp. 466–471.

[14] W. Baxter, E. Aboutanios, and A. Hassanien, "Dual-function MIMO radar-communications via frequency-hopping code selection," in *2018 52nd Asilomar Conf. on Signals, Syst., and Computers*, Oct 2018, pp. 1126–1130.

[15] I. P. Eedara and M. G. Amin, "Performance comparison of dual-function systems embedding phase-modulated signals in fh radar (conference presentation)," in *Signal Processing, Sensor/Information Fusion, and Target Recognition XXIX*, vol. 11423. International Society for Optics and Photonics, 2020, p. 114230U.

[16] K. Wu, Y. J. Guo, X. Huang, and R. W. Heath, "Accurate channel estimation for frequency-hopping dual-function radar communications," in *2020 IEEE International Conference on Communications Workshops (ICC Workshops)*, 2020, pp. 1–6.

[17] K. Wu *et al.*, "Waveform design and accurate channel estimation for frequency-hopping MIMO radar-based communications," *IEEE Trans. Commun., early access*, 2020.

[18] K. Wu, J. A. Zhang, X. Huang, and Y. J. Guo, "Integrating secure and high-speed communications into frequency hopping MIMO radar," *arXiv preprint arXiv:2009.13750*, 2020.

[19] X. Huang, J. A. Zhang, R. P. Liu, Y. J. Guo, and L. Hanzo, "Airplane-aided integrated networking for 6G wireless: Will it work?" *IEEE Veh. Technol. Mag.*, vol. 14, no. 3, pp. 84–91, 2019.

[20] Y. Zeng, Q. Wu, and R. Zhang, "Accessing from the sky: A tutorial on UAV communications for 5G and beyond," *Proc. IEEE*, vol. 107, no. 12, pp. 2327–2375, 2019.

[21] M. K. Simon and M.-S. Alouini, *Digital communication over fading channels*. John Wiley & Sons, 2005.

[22] Y. Zhang, Ling Huang, and Jian Song, "Phased array radar based angular domain channel estimation scheme for integrated radar-communication system," in *MILCOM 2016*, 2016, pp. 906–911.

[23] L. Huang, Y. Zhang, Q. Li, and J. Song, "Phased array radar-based channel modeling and sparse channel estimation for an integrated radar and communication system," *IEEE Access*, vol. 5, pp. 15 468–15 477, 2017.

[24] A. Serbes, "Fast and efficient sinusoidal frequency estimation by using the DFT coefficients," *IEEE Trans. Commun.*, vol. 67, no. 3, pp. 2333–2342, March 2019.

[25] K. Wu, W. Ni, J. A. Zhang, R. P. Liu, and Y. J. Guo, "Refinement of optimal interpolation factor for DFT interpolated frequency estimator," *IEEE Commun. Lett.*, pp. 1–1, 2020.

[26] N. Su, F. Liu, and C. Masouros, "Secure radar-communication systems with malicious targets: Integrating radar, communications and jamming functionalities," *IEEE Trans. Wireless Commun.*, pp. 1–1, 2020.

[27] J. M. Hamamreh, H. M. Furqan, and H. Arslan, "Classifications and applications of physical layer security techniques for confidentiality: A comprehensive survey," *IEEE Commun. Surveys Tuts.*, vol. 21, no. 2, pp. 1773–1828, 2019.

[28] M. E. Eltayeb, J. Choi, T. Y. Al-Naffouri, and R. W. Heath, "Enhancing secrecy with multiantenna transmission in millimeter wave vehicular communication systems," *IEEE Trans. Vehicular Technology*, vol. 66, no. 9, pp. 8139–8151, 2017.

[29] Y. L. Sit, B. Nuss, S. Basak, M. Orzol, W. Wiesbeck, and T. Zwick, "Real-time 2d+velocity localization measurement of a simultaneous-transmit OFDM MIMO radar using software defined radios," in *2016 European Radar Conference (EuRAD)*, 2016, pp. 21–24.

[30] M. T. Frankford, N. Majurec, and J. T. Johnson, "Software-defined radar for mimo and adaptive waveform applications," in *2010 IEEE Radar Conference*, 2010, pp. 724–728.